Pulsar wind nebulae of runaway massive stars

D. M. -A. Meyer, Z. Meliani

Monthly Notices of the ROYAL ASTRONOMICAL SOCIETY
MNRAS **515,** L29–L33 (2022) https://doi.org/10.1093/mnrasl/slac062

Pulsar wind nebulae of runaway massive stars

D. M.-A. Meyer [1]★ and Z. Meliani [2]

[1] *1Institut für Physik und Astronomie, Universität Potsdam, Karl-Liebknecht-Strasse 24/25, D-14476 Potsdam, Germany*
[2] *2Laboratoire Univers et Théories, Observatoire de Paris, Université PSL, Université de Paris, CNRS, F-92190 Meudon, France*

Accepted 2022 June 8. Received 2022 June 8; in original form 2022 May 10

ABSTRACT

A significant fraction of massive stars move at speed through the interstellar medium of galaxies. After their death as core-collapse supernovae, a possible final evolutionary state is that of a fast-rotating magnetized neutron star, shaping its circumstellar medium into a pulsar wind nebula. Understanding the properties of pulsar wind nebulae requires knowledge of the evolutionary history of their massive progenitors. Using two-dimensional magnetohydrodynamical simulations, we demonstrate that, in the context of a runaway high-mass red-supergiant supernova progenitor, the morphology of its subsequent pulsar wind nebula is strongly affected by the wind of the defunct progenitor star pre-shaping the stellar surroundings throughout its entire past life. In particular, pulsar wind nebulae of obscured runaway massive stars harbour asymmetries as a function of the morphology of the progenitor's wind-blown cavity, inducing projected asymmetric up–down synchrotron emission.

Key words: methods: MHD – stars: evolution – stars: massive – pulsars: general – ISM: supernova remnants.

1 INTRODUCTION

About 10 per cent to 25 per cent of OB-type massive stars are runaway objects (Blaauw 1961; Schoettler, Parker & de Bruijne 2022) with peculiar supersonic speeds with respect to their interstellar medium (ISM). Two main mechanisms are proposed to explain the production of such runaway stars, namely binary-supernova ejection and dynamical ejection from the stellar cluster (Hoogerwerf, de Bruijne & de Zeeuw 2000), and their trajectories can be traced back to their parent starburst regions (Schoettler et al. 2019). These massive stars die as core-collapse supernovae, releasing most of the remaining stellar mass at high speed into the surrounding circumstellar medium (CSM) before expanding into the ISM.

Often, at the location of the supernova explosion, there remains a highly magnetized and fast-rotating neutron star (a pulsar). The pulsar generates a powerful wind with a kinetic luminosity that can reach $\dot{E} \sim 10^{39}\,\mathrm{erg\,s^{-1}}$, inducing a growing pulsar wind nebula (PWN). This PWN evolves first into freely expanding supernova ejecta before reaching the supernova reverse shock (Blondin, Chevalier & Frierson 2001). After this, it interacts with the swept-up CSM and, at a later time, with the unshocked ISM.

Previous investigations on PWNe of moving pulsars have concentrated on the birth kick pulsar. This occurs when massive stars collapse (de Vries et al. 2021). The resulting pulsar propagates through the supernova ejecta (Slane et al. 2018). On time-scales of a few kyr, the fast-moving pulsar escapes the supernova remnant (SNR) and travels in the uniform and cold ISM (Barkov et al. 2019; Bucciantini, Olmi & Del Zanna 2020). The resulting PWN morphology is strongly deformed and develops an extended tail. Because of numerical and physical difficulties associated with the CSM modelling, the simulations of PWNe are mainly performed in classical hydrodynamics and deal only with moving pulsars inside supernova ejecta (Temim et al. 2015, 2022). Relativistic simulations have been performed for pulsars moving in the ISM (Barkov et al. 2019; Bucciantini et al. 2020), while others also deal with static pulsar winds expanding into the supernova ejecta in 1D and 2D (Blondin et al. 2001; van der Swaluw et al. 2003; van der Swaluw 2003; van der Swaluw, Downes & Keegan 2004; Slane et al. 2018). However, these works did not account for all the evolutionary phases of the stellar progenitor of the runaway pulsar.

For pulsars from massive runaway stars, their winds mainly expand in supernova remnant (SNRs) constituted of supernova ejecta and CSM materials. Thus, shocks and instabilities, as well as the overall PWN morphology, will be affected by these structures. Since SNRs are strongly affected by the CSM distribution (Cox et al. 2012), the PWNe and the properties of the various shocks therein should be, in turn, a function of the surrounding CSM. Most commonly, runaway massive stars shape the CSM with a large amount of red-supergiant material as dense asymmetric stellar-wind bow shocks (Cox et al. 2012; Henney & Arthur 2019a, b, c; Meyer, Petrov & Pohl 2020a; Herbst et al. 2022), so this should not be omitted in the modelling of their PWN.

Motivated by the above arguments, we numerically investigate the shaping of the PWN of a fast-moving massive core-collapse supernova progenitor. We focus on the particular effects of the CSM generated by the wind–ISM interaction of the progenitor star. This study is organized as follows. First, we present the numerical methods used to model the pulsar wind nebula of a runaway massive progenitor star in Section 2. The outcomes of the simulations are presented in Section 3. We discuss our results and draw our conclusions in Section 4.

2 METHOD

This study focuses on the entire evolution of the circumstellar medium of a runaway 20 $\mathrm{M}_\odot$ star at Galactic metallicity. The stellar surface properties such as wind velocity and mass-loss rate histories

★ E-mail: dmameyer.astro@gmail.com

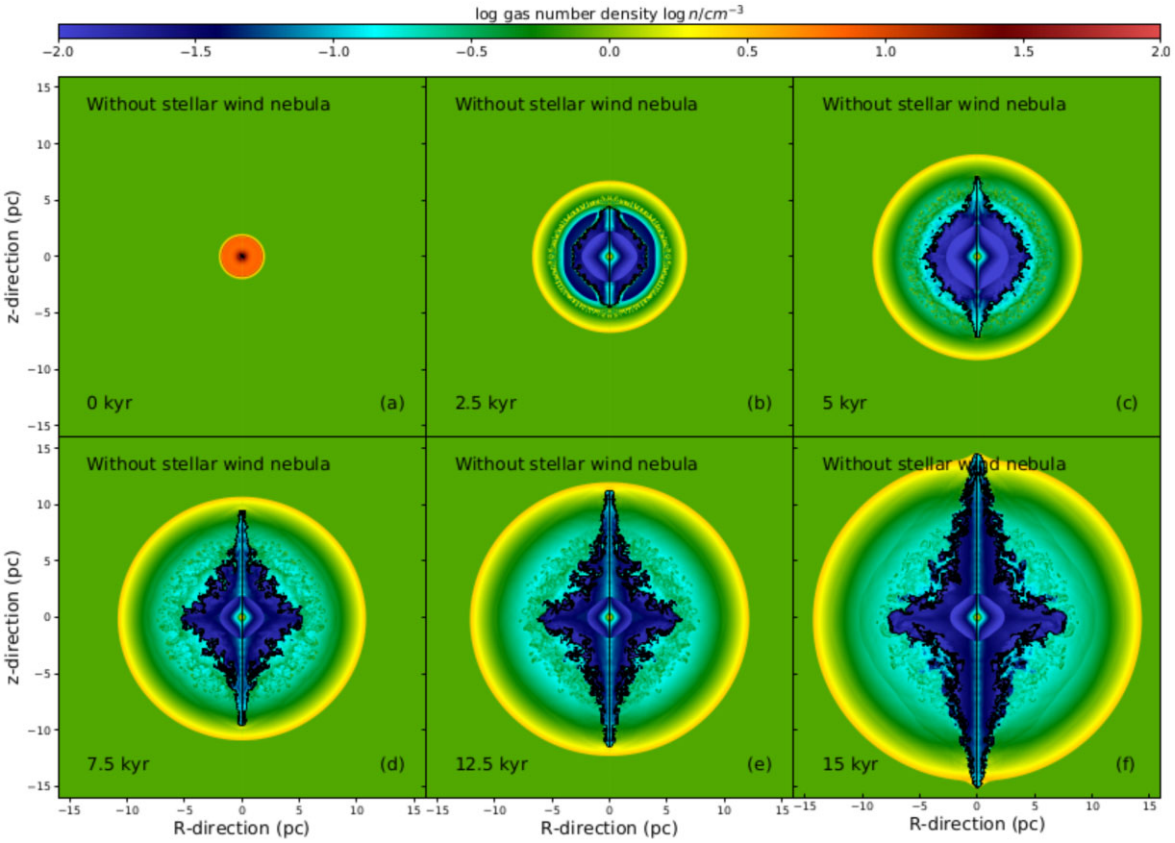

Figure 1. Time evolution of the number density field (in cm^{-3}) in the simulation of the nebula generated by a pulsar wind injected into the expanding ejecta of a core-collapse supernova. The black contour marks the region of the nebula made of 50 per cent of pulsar wind material in number density. Time is measured starting from the onset of the pulsar wind.

are taken from a model of the GENEVA evolutionary tracks library calculated without rotational mixing (Eldridge et al. 2006; Ekström et al. 2012).

We model the stellar surroundings from the zero-age main-sequence to the pre-supernova phase, through its red-supergiant phase. When the star achieves its evolution, we inject therein supernova core-collapse ejecta made of mass $M_{\rm ej} = 6.96\,\mathrm{M}_\odot$ and energy $E_{\rm ej} = 10^{51}$ erg, using a density power-law profile (Whalen et al. 2008; Meyer et al. 2020a). The pulsar wind is modelled according to Komissarov & Lyubarsky (2004), using a wind power $\dot{E}_{\rm o} = 10^{38}\,\mathrm{erg\,s}^{-1}$, a wind velocity $10^{-2}c$ with c the speed of light in vacuum, a pulsar spin $P_{\rm o} = 0.3$ s, a spin period variation $\dot{P}_{\rm o} = 10^{-17}\,\mathrm{s\,s}^{-1}$, and a wind magnetization parameter $\sigma = 10^{-3}$ (Slane 2017). The pulsar loses energy according to an initial spin-down time-scale $\tau_{\rm o} = P_{\rm o}/((N-1)\dot{P}_{\rm o})$, where the braking index $N = 3$ stands for magnetic dipole spin-down. The energy diminution equation therefore reads $\dot{E}(t) = \dot{E}_{\rm o}(1 + t/\tau_{\rm o})^{\alpha}$ with $\alpha = -(N+1)/(N-1)$; see Pacini & Salvati (1973). In this first paper, we run 2.5D simulations. Therefore, it is assumed that the spin axis and the direction of motion of the star coincide with the axis of symmetry of the cylindrical coordinate system.

The massive star moves through the ISM of the Milky Way's Galactic plane of initial gas density $0.79\,\mathrm{cm}^{-3}$ and temperature 8000 K (Wolfire et al. 2003; Meyer et al. 2014). We adopt an undisturbed ISM magnetic field parallel to the direction of motion of the star with a strength of 7 μG, which corresponds to an Alfvén speed of $v_{\rm A} = 17.2\,\mathrm{km\,s}^{-1}$ (Meyer et al. 2017).

The 2.5D numerical magnetohydrodynamical simulations are performed with the code PLUTO (Mignone et al. 2007, 2012). We make use of the Godunov-type numerical scheme HLL Riemann solver combined with the PPM limiter, together with a third-order Runge–Kutta time-marching algorithm controlled by the Courant–Friedrich–Levi number. As in van der Swaluw et al. (2003), we set the polytropic index to 5/3 and optically thin radiative cooling physics is used for all circumstellar evolutionary phases except when starting from the onset of the pulsar wind. More precisely, we make use of the optically thin cooling and heating curves for a fully ionized medium (Wiersma, Schaye & Smith 2009) of solar abundance (Asplund et al. 2009) presented in Meyer et al. (2014). Calculations are conducted following a mapping strategy (van Marle, Meliani & Marcowith 2015; Meyer et al. 2020a, 2021) in which the progenitor's CSM is first calculated, before supernova ejecta and eventually pulsar wind are injected into it. The models are conducted using a cylindrical coordinate system (R, z) that is mapped with a uniform mesh $[0, 150] \times [-50, 50]$ of spatial resolution $1.2 \times 10^{-2}\,\mathrm{pc\,cell}^{-1}$ for the CSM and a mesh $[0, 20] \times [-20, -20]$ of resolution $6.7 \times 10^{-3}\,\mathrm{pc\,cell}^{-1}$ for the PWN. The central sphere in which winds are imposed is of radius 20 cells (0.24 pc during the stellar-wind phase and 0.134 pc throughout the pulsar phase).

Two simulations are performed with a runaway star of space velocity $v_\star = 40\,\mathrm{km\,s}^{-1}$ (Mach number $\mathcal{M} \sim 4$). The first one considers the pulsar wind expanding into supernova ejecta only, while the second one also accounts for the progenitor's CSM.

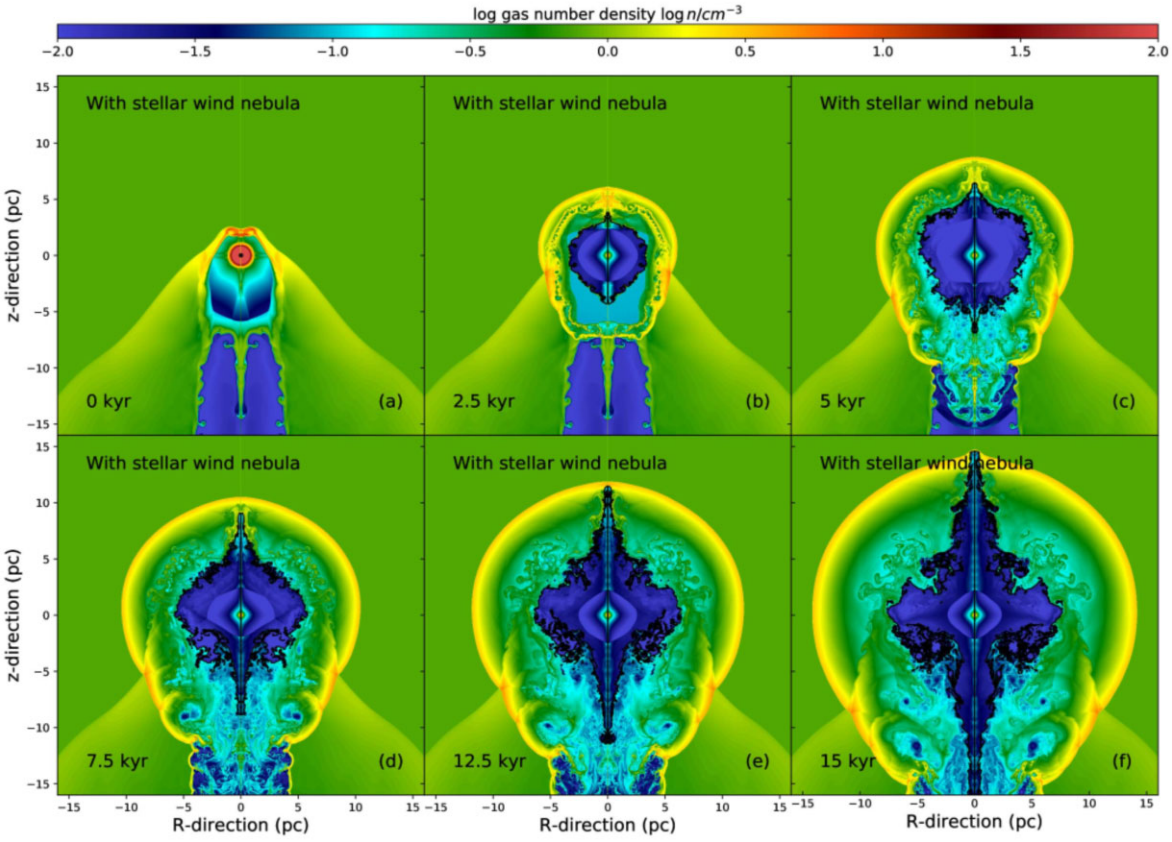

Figure 2. As for Fig. 1, with the presence of the circumstellar medium (CSM) generated by the wind–ISM interaction of the 20 $M_\odot$ massive runaway progenitor.

3 RESULTS

3.1 Model without wind–ISM interaction

For the sake of comparison, we first model a PWN accounting for core-collapse supernova ejecta but neglecting the CSM, the entire system being in supersonic motion in the ambient medium. The time sequence of the evolution of the number density field of such a system is displayed in Fig. 1.

The pulsar wind is set in the dense supernova ejecta that has expanded up to a few pc into the local ISM (Fig. 1a). About 2.5 kyr later, the PWN has adopted a structure made of the freely expanding pulsar wind, a PWN termination shock, a PWN/ejecta inner contact discontinuity (black contour), and a transmitted PWN forward shock propagating into the unshocked supernovae ejecta. The ejecta–ISM interaction leads to the formation of an outer ejecta–ISM contact discontinuity affected by strong Richtmyer–Meshkov instabilities (Kane, Drake & Remington 1999), while a reflected supernova termination shock forms and propagates inwards, heating the pulsar wind. Meanwhile, the supernova forward shock propagates through the ISM (Fig. 1b).

The system keeps on growing in size over the next few kyr, revealing an efficient mixing of pulsar and ejecta materials. The magnetized pulsar wind develops a bipolar jet along its rotation axis; see the black contours of Fig. 1(c). At time 7.5 kyr the PWN harbours an equatorial disc-like feature, normal to the bipolar jet, which has gone through the unstable region where the mixing of materials takes place and penetrates the outer layer of shocked ISM gas of the SNR (Fig. 1d). The magnetized PWN, at this point, displays the typical cross-like anisotropic morphology described in Komissarov & Lyubarsky (2004), embedded by an overall spherically symmetric expanding blastwave (Fig. 1e). Lastly, the jet of the pulsar catches up with the supernova remnant shock wave and begins to expand into the ISM, generating polar bow shocks (Fig. 1f).

During the evolution, the high speed of the supernova ejecta compensates the ISM ram pressure, allowing the SNR, and consequently the PWN morphology, to conserve an isotropic symmetry.

3.2 Effects of the progenitor's wind–ISM interaction

In the second model, all evolutionary stages of the massive progenitor are considered before the supernova explosion occurs and the pulsar starts blowing into the former stellar wind (Fig. 2). The gas distribution at the onset of the pulsar wind is complex, as the wind–ISM interaction has shaped it throughout the previous star's life. Its arc-like nebula is composed of a large-scale component produced by the main-sequence stellar wind plus the shell of the red-supergiant wind that has been subsequently released in it (Meyer et al. 2014). The pre-pulsar CSM is therefore a central region of expanding ejecta surrounded by a low-density cavity , with a high-density bow shock facing the direction of the progenitor's motion (Fig. 2a); see also Meyer et al. (2015, 2021). The asymmetric propagation of the supernova blastwave is strongly constrained by the walls of the cavity. It is channelled by the cavity in the direction opposite to that in which the stellar motion shock has gone through the CSM (Fig. 2b).

The global organization of the SNR and its central PWN exhibits qualitative dissimilarities to that of Fig. 1 as the gameof shock reflections generates a more complex object. The morphology of

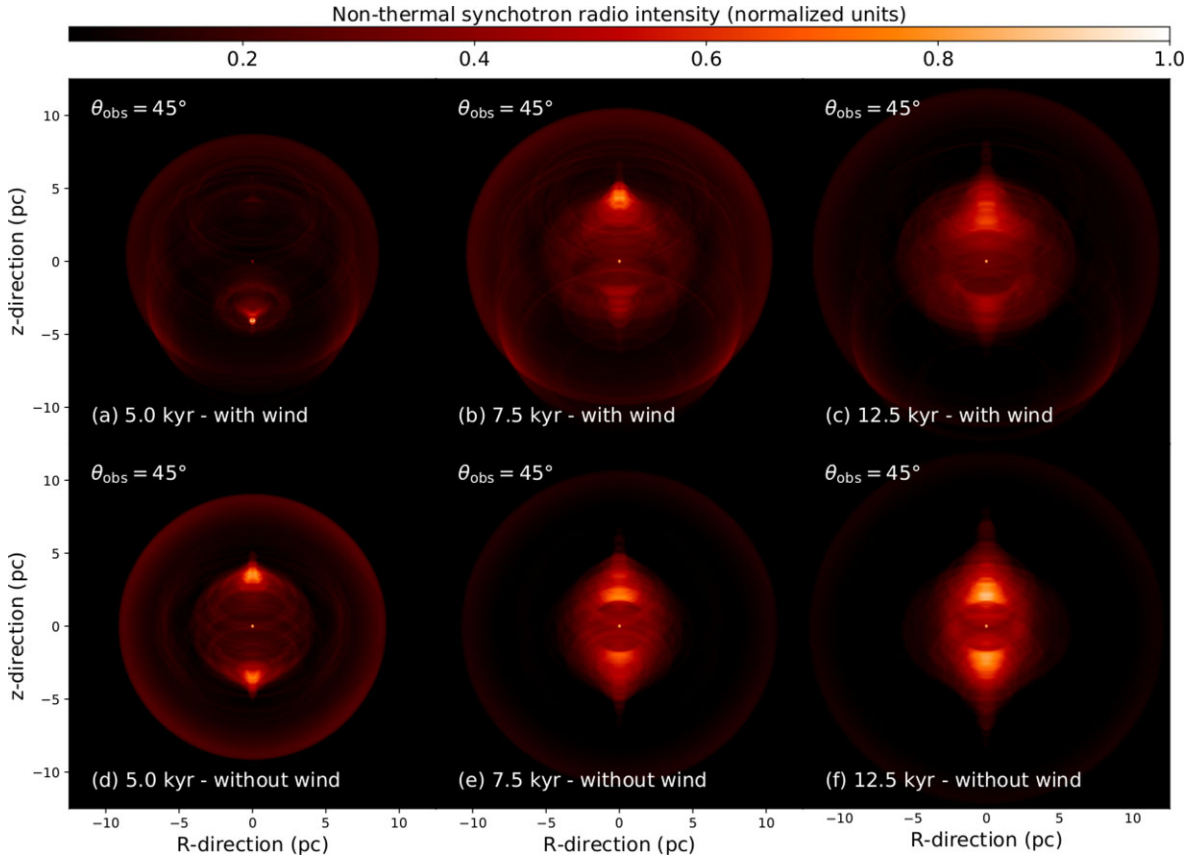

Figure 3. Selected time-sequence evolution of the synchrotron emission map assuming an angle $\theta_{\rm obs} = 45^\circ$ between the observer's line of sight and the axis of symmetry of the nebula. The images compare models with (top) and without (bottom) the stellar wind of the massive progenitor.

the pulsar wind–ejecta interface is governed by that of the ejecta region, adopting an ovoidal shape (Fig. 2c) different to that of the model without the progenitor's stellar wind (Fig. 1c). At the time 7.5 kyr, the supernova ejecta are channelled into the tubular region of shocked stellar wind generated by the progenitor's motion and the pulsar wind develops a bipolar jet, although the pulsar wind remains equatorially asymmetric (Fig. 2d). The nebula further evolves such that the inner contact discontinuity of the PWN is shaped as a function of (i) the pulsar magnetorotational properties and (ii) the supernova shock wave material that is reflected towards the centre of the explosion. Finally, the contact discontinuity recovers the overall morphology of a bipolar jet normal to an equatorial structure (Fig. 2e), with important persisting equatorial dissymmetries (Fig. 2f).

4 DISCUSSION AND CONCLUSION

In this paper, we numerically investigate, in the context of a runaway massive supernova progenitor and within the frame of the ideal magnetohydrodynamics, the influences of the CSM shape during all the progenitor's evolutionary stages on the long-term ($\sim$ kyr) morphological development of the PWN after the pulsar birth and on the instabilities growing at shocks. Other works concerning the release of pulsar winds in SNRs were set in the frame of ideal hydrodynamics (Blondin et al. 2001; van der Swaluw et al. 2003; van der Swaluw 2003; van der Swaluw et al. 2004; Slane et al. 2018) as well as magnetohydrodynamics; see Olmi & Torres (2020) and references therein. Nevertheless, although some studies have tackled the problem of runaway pulsars (Olmi & Bucciantini 2019), or even investigated the effects of a stratified ISM (Kolb et al. 2017), none of them include in detail the stellar-wind feedback of the core-collapse progenitor. In our scenario, the pulsar wind–supernova ejecta system is embedded into a dense CSM, where a large part of the progenitor mass lies, released as a pre-supernova stellar wind. Note that our models assume that the pulsar is static in the frame of reference of the runaway star, so we are neglecting the birth kick that many pulsars receive from the supernova explosion. Assuming a typical kick velocity of $\approx 400\,{\rm km\,s^{-1}}$ (Verbunt, Igoshev & Cator 2017), the pulsar would be displaced by about 6 pc over the 15 pc that we simulate. Therefore our results apply mainly to the low-velocity pulsar sub-population ($\leq 50\,{\rm km\,s^{-1}}$), which comprises $\approx$ 2–5 per cent of all pulsars (Igoshev 2020).

Our study shows, in the particular context of a fast-moving red-supergiant star in the Galactic plane, that the wind-blown bubble of a core-collapse supernova progenitor has a governing impact on the morphology of its subsequent PWN. As early as $\sim$ 2.5 kyr, the distribution of the contact discontinuity between a magnetized pulsar wind and the supernova ejecta adopts an oblong shape as a result of the anisotropic ejecta distribution. Since core-collapse SNRs are shaped according to their CSM, PWNe similarly take their morphology as a direct consequence of their progenitor's stellar evolution history. Because a significant fraction of massive stars are runaway objects, our findings imply that the stellar-wind history should not be neglected in the understanding of PWNe and that the CSM-induced asymmetries should account for up to 10 per cent to 25 per cent of all individual PWNe.

The stellar-wind history that we use is that of a $20\,M_\odot$ supergiant star, which is amongst the most common progenitors of core-collapse SNRs (Katsuda et al. 2018), although higher-mass evolutionary channels might exist, i.e. involving Wolf–Rayet progenitors. The bulk motion of the star is taken to be within that of the most common runaway stars (Blaauw 1993). However, a small fraction of high-mass stars move with very high velocities (Lennon et al. 2018) and might form PWNe, for which the influence of the CSM is milder. Given that the morphology of PWNe retains information from the stellar evolution history of massive stars, our model applies to objects in the Galactic disc region ($\sim 1\,\mathrm{cm}^{-3}$) rather than in the high-latitude parts of the Milky Way, where the low-density medium induces an extended CSM (Meyer et al. 2020b) with which supernova shock waves (and eventually pulsar winds) weakly interact. Conversely, massive stars running through dense molecular regions are more likely to form complex CSM and, therefore, to produce very asymmetric PWNe.

We generate predictive images for our asymmetric PWN from a runaway massive star. Fig. 3 plots non-thermal radio synchrotron emission maps using the emissivity $\propto p B_\perp^{(s+1)/2}$ with p the thermal pressure of the gas, $B_\perp$ the component of the magnetic field along the observer's line of sight, and $s = 2$ the power-law index of the non-thermal electron distribution (Jun & Norman 1996). The images are produced with the RADMC-3D code (Dullemond 2012), displayed with (top) and without (bottom) CSM, for selected time instances, and assuming an inclination angle of the pulsar of $\theta_{\rm obs} = 45^\circ$ to the plane of the sky. The pulsar wind is at first not visible in the region facing the progenitor's direction of motion, where the supernova shock wave interacting with the wind bubble dominates (Figs 3a, d). Once the pulsar polar jet grows and penetrates the dense region of stellar wind and ejecta, it becomes brighter than that in the cavity (Figs 3b, c). This projected up–down surface brightness asymmetry increases with time, as the front jet starts to interact with the shocked supernova material and the jet on the other side continues to propagate in the rarefied medium of the stellar-wind cavity.

Our results show that the effects of the progenitor's stellar wind impacts the global morphology of PWNe and consequently influences the properties of the shocks therein. This should significantly modify the injection and acceleration physics of the relativistic particle population, which, in turn, is responsible for the non-thermal emission properties of PWNe.

We intend to extend this work to a broader study, investigating the parameter space of various massive stellar progenitors, treating the pulsar wind relativistically, and including the kick received by a pulsar.

ACKNOWLEDGEMENTS

The authors thank the referee, W. Henney, for advice that improved the quality of the paper. The authors acknowledge the North-German Supercomputing Alliance (HLRN) for providing HPC resources that have contributed to the research results reported in this paper.

DATA AVAILABILITY

The data underlying this article will be shared on reasonable request to the corresponding author.

REFERENCES

Asplund M., Grevesse N., Sauval A. J., Scott P., 2009, ARA&A, 47, 481
Barkov M. V., Lyutikov M., Klingler N., Bordas P., 2019, MNRAS, 485, 2041
Blaauw A., 1961, Bull. Astron. Inst. Netherlands, 15, 265
Blaauw A., 1993, in Cassinelli J. P., Churchwell E. B., eds, ASP Conf. Ser. Vol. 35, Massive Stars: Their Lives in the Interstellar Medium. Astron. Soc. Pac., San Francisco, p. 207
Blondin J. M., Chevalier R. A., Frierson D. M., 2001, ApJ, 563, 806
Bucciantini N., Olmi B., Del Zanna L., 2020, J. Phys. Conf. Ser., 1623, 012002
Cox N. L. J., Kerschbaum F., van Marle A.-J., Decin L., Ladjal D., Mayer A., 2012, A&A, 537, A35
de Vries M. et al., 2021, ApJ, 908, 50
Dullemond C. P., 2012, Astrophysics Source Code Library, record ascl:1202.015
Ekström S. et al., 2012, A&A, 537, A146
Eldridge J. J., Genet F., Daigne F., Mochkovitch R., 2006, MNRAS, 367, 186
Henney W. J., Arthur S. J., 2019a, MNRAS, 486, 3423
Henney W. J., Arthur S. J., 2019b, MNRAS, 486, 4423
Henney W. J., Arthur S. J., 2019c, MNRAS, 489, 2142
Herbst K. et al., 2022, Space Sci. Rev., 218, 29
Hoogerwerf R., de Bruijne J. H. J., de Zeeuw P. T., 2000, ApJ, 544, L133
Igoshev A. P., 2020, MNRAS, 494, 3663
Jun B.-I., Norman M. L., 1996, ApJ, 472, 245
Kane J., Drake R. P., Remington B. A., 1999, ApJ, 511, 335
Katsuda S., Takiwaki T., Tominaga N., Moriya T. J., Nakamura K., 2018, ApJ, 863, 127
Kolb C., Blondin J., Slane P., Temim T., 2017, ApJ, 844, 1
Komissarov S. S., Lyubarsky Y. E., 2004, MNRAS, 349, 779
Lennon D. J. et al., 2018, A&A, 619, A78
Meyer D. M.-A., Mackey J., Langer N., Gvaramadze V. V., Mignone A., Izzard R. G., Kaper L., 2014, MNRAS, 444, 2754
Meyer D. M.-A., Langer N., Mackey J., Velázquez P. F., Gusdorf A., 2015, MNRAS, 450, 3080
Meyer D. M.-A., Vorobyov E. I., Kuiper R., Kley W., 2017, MNRAS, 464, L90
Meyer D. M. A., Petrov M., Pohl M., 2020a, MNRAS, 493, 3548
Meyer D. M. A., Oskinova L. M., Pohl M., Petrov M., 2020b, MNRAS, 496, 3906
Meyer D. M. A., Pohl M., Petrov M., Oskinova L., 2021, MNRAS, 502, 5340
Mignone A., Bodo G., Massaglia S., Matsakos T., Tesileanu O., Zanni C., Ferrari A., 2007, ApJS, 170, 228
Mignone A., Zanni C., Tzeferacos P., van Straalen B., Colella P., Bodo G., 2012, ApJS, 198, 7
Olmi B., Bucciantini N., 2019, MNRAS, 488, 5690
Olmi B., Torres D. F., 2020, MNRAS, 494, 4357
Pacini F., Salvati M., 1973, ApJ, 186, 249
Schoettler C., Parker R. J., Arnold B., Grimmett L. P., de Bruijne J., Wright N. J., 2019, MNRAS, 487, 4615
Schoettler C., Parker R. J., de Bruijne J., 2022, MNRAS, 510, 3178
Slane P., 2017, in Alsabti A. W., Murdin P., eds, Handbook of Supernovae, p. 2159
Slane P. et al., 2018, ApJ, 865, 86
Temim T., Slane P., Kolb C., Blondin J., Hughes J. P., Bucciantini N., 2015, ApJ, 808, 100
Temim T., Slane P., Raymond J. C., Patnaude D., Murray E., Ghavamian P., Renzo M., Jacovich T., 2022, ApJ, 932, 26
van der Swaluw E., 2003, A&A, 404, 939
van der Swaluw E., Achterberg A., Gallant Y. A., Downes T. P., Keppens R., 2003, A&A, 397, 913
van der Swaluw E., Downes T. P., Keegan R., 2004, A&A, 420, 937
van Marle A. J., Meliani Z., Marcowith A., 2015, A&A, 584, A49
Verbunt F., Igoshev A., Cator E., 2017, A&A, 608, A57
Whalen D., van Veelen B., O'Shea B. W., Norman M. L., 2008, ApJ, 682, 49
Wiersma R. P. C., Schaye J., Smith B. D., 2009, MNRAS, 393, 99
Wolfire M. G., McKee C. F., Hollenbach D., Tielens A. G. G. M., 2003, ApJ, 587, 278

This paper has been typeset from a TEX/LATEX file prepared by the author.